Primljen / Received: 6.7.2021.
Ispravljen / Corrected: 20.9.2021.
Prihvaćen / Accepted: 30.11.2021.
Dostupno online / Available online: 10.1.2022.

An approach for dynamic analysis of steel plate shear wall systems

Autohrs:

Yasin Gungor, Bsc
Canakkale Onsekiz Mart University, Turkey
Faculty of Engineering
Department of Civil Engineering
ysngungor@outlook.com

Prof. **Kanat Burak Bozdogan**, PhD. CE
Canakkale Onsekiz Mart University, Turkey
Faculty of Engineering
Department of Civil Engineering
kbbozdogan@comu.edu.tr
Corresponding author

Research Paper

Yasin Gungor, Kanat Burak Bozdogan

An approach for dynamic analysis of steel plate shear wall systems

In this paper, the Timoshenko beam model (continuous system model) is originally adapted for dynamic analysis of steel plate shear wall (SPSW) systems. Dynamic characteristics for the first three modes are found by solving differential equation of the equivalent Timoshenko beam model using the differential transformation method. Dynamic characteristics are tabulated for quick and practical calculation. With the help of the dynamic characteristics, the response spectrum analysis of such buildings is performed. Using the approach developed in this study, it is possible to calculate not only natural periods, but also the base shear force, maximum storey displacement, and maximum storey drift ratio. The differential transformation method is used in this study for solving the differential equation written according to the continuous system calculation model. To investigate the suitability of the method presented in the study, an example taken from the literature is solved and the results are evaluated. The results show that the method presented can be used in the preliminary design stage.

Key words:
steel plate shear wall, continuum model, Timoshenko beam, differential transform method, dynamic characteristics

Prethodno priopćenje

Yasin Gungor, Kanat Burak Bozdogan

Dinamička analiza posmičnih stijena s čeličnom ispunom

U ovom se radu prikazuje model Timošenkove grede (model za kontinuirane sustave) koji je na originalan način prilagođen za provedbu dinamičke analize sustava posmičnih stijena s čeličnom ispunom (SPSW). Dinamičke karakteristike za prva tri oblika izračunane su rješavanjem diferencijalne jednadžbe modela ekvivalentne Timošenkove grede primjenom metode diferencijalne transformacije. Dinamičke karakteristike prikazane su tablično kako bi se omogućilo brzo i praktično izračunavanje. Pomoću dinamičkih karakteristika provedena je analiza spektra odziva takvih građevina. Primjenom pristupa razvijenog u ovom istraživanju mogu se izračunani ne samo osnovni periodi već i posmična sila na razini tla, maksimalni katni pomak i maksimalni relativni katni pomak. Metoda diferencijalne transformacije u ovoj se radu koristi za rješavanja diferencijalne jednadžbe iskazane prema proračunskom modelu za kontinuirane sustave. Kako bi se ispitala pogodnost metode prezentirane u radu, riješen je primjer iz literature, te je provedeno ocjenjivanje dobivenih rezultata. Rezultati pokazuju da se prikazana metoda može koristiti u preliminarnom koraku projektiranja građevina.

Ključne riječi:
posmična stijena s čeličnom ispunom, model kontinuuma, Timošenkova greda, metoda diferencijalne transformacije, dinamičke karakteristike

1. Introduction

To prevent building damage under earthquake loads, storey displacements and the storey drift ratios must remain below certain limit values. One of the systems used for limiting the displacement and drift ratio in steel buildings is the steel plate shear wall (SPSW) system.

In recent years, many experimental and analytical studies have been conducted to determine behaviour of steel buildings using such systems. Some of these studies are briefly summarized below.

Love et al. [1], used SPSW systems to strengthen a steel-framed hospital building damaged in the 1994 Northridge Earthquake. In the study, the authors show that strengthening with SPSW provides the desired level of compliance with relevant standards.

Berman et al. [2], investigated damage conditions of SPSW systems and suggested repair methods. As a result of the study, a database was created for systems using steel plate shear walls.

Bhowmick et al. [3], proposed a capacity design method for SPSW systems that enables better seismic performance at moderate cost. The method proposed in the study was proven to be compatible with the results of nonlinear analysis.

Clayton et al. [4] proposed a design procedure for self-centring SC-SPSW systems developed using a performance-based design approach. The study shows that SC-SPSW systems perform well at three distinct earthquake levels.

Clayton et al. [5], studied behaviour of self-centring SPSW systems under cyclic loading. The experiments carried out in the study show that the SC-SPSW system exhibits a high level of ductility and rigidity.

Alavi and Nateghi [6] showed that the response modification factor (R) of diagonally stiffened SPSW systems is approximately 13% greater than that of un-stiffened systems. They observed that especially the use of edge stiffeners in plates improves hysteretic behaviour of SPSW.

Nie et al. [7], experimentally investigated seismic behaviour of the perforated and non-perforated stiffened SPSW systems. As a result of the experiments, they recommended the use of stiffened plates to increase the decreasing strength and stiffness of perforated SPSW.

Dowden and Bruneau [8] modelled self-centring SPSW systems in full scale and compared them with analytical results. At the end of the study, they demonstrated that the proposed analytical method is compatible with the experimental results.

Dowden et al. [9] investigated a self-centring SPSW system on a full scale to limit the damage in SPSW systems. As a result of the experiments carried out in the study, it was established that the self-centring steel plate shear walls systems provided the desired performance. Yu et al. [10], investigated cyclic performance of cross restrained steel plate shear walls with transverse braces. As a result of the experiments, it was established that cyclic performance of the proposed system is higher than that of the classical system.

Wang and Xie [11], proposed a concrete-filled steel tubular column (CFST) and cross-reinforced SC-SPSW against the buckling of the H-section steel column base and the pinching effect in hysteretic curves, which are two main problems in thin SC-SPSWs. As a result of the experiments and analytical solutions, it was concluded that the proposed system increased yield load and maximum load.

Barua and Bhowmick [12], examined nonlinear seismic performances of perforated SPSW systems designed according to the seismic code. In the study, it was observed that the perforated steel plate shear walls systems performed well in terms of ductility and strength.

Curkovic et al. [13], studied behaviour of SPSW with variable flexural stiffness columns experimentally and numerically. At the end of the study, it was emphasized that the minimum column bending stiffnesses in AISC 341-10 may be too conservative.

Bai et al. [14], proposed a simplified seismic design method to improve performance for low-rise dual-frame SPSW structures. In the study, low-rise dual-frame SPSW structures are reduced to an equivalent single degree of freedom system. As a result of the analysis, it was established that the proposed single degree of freedom model properly represented behaviour of the system.

Azarafrooz and Shekastehband [15] investigated behaviour of the 4- and 8-storey SPSW infill plate connected to the frame in three different ways. The study shows that secondary columns provide a remarkable increase in the shear capacity of the system.

Fathy [16] investigated behaviour of frame SPSW buildings without and with outriggers. Nonlinear analyses were carried out in the study using the finite element method. At the end of the study, it was seen that the system with two outriggers performed better than the system with one outrigger. It was also emphasized in the study that lateral displacements decreased with an increase in the number of outriggers.

Liu He, and Li [17] experimentally investigated hysteretic behaviour of the SPSW system with self-centring energy dissipation braces. At the end of the study, it was concluded that the compressive bearing capacity of the wall plate should be smaller than the horizontal resting force of the braces to increase the self-centring effect of the system.

Jiang et al. [18], proposed a formula for calculating fundamental periods of SPSW systems. In the development of the proposed formula, it was accepted that the steel frame showed shear behaviour, whereas the plate shear walls showed flexural and shear behaviour. The suitability of the analytical method presented at the end of the study was demonstrated through appropriate examples.

Zhao et al. [19], investigated suitability of the empirical period relationship used in the corrugated steel plate shear wall systems and proposed a formula for calculating period of such systems by using the shear-flexural beam model. As a result of the study, it was established that the proposed analytical method gives results close to those obtained by the finite element method.

In this study, unlike the literature, the equivalent continuous Timoshenko beam model was used for the dynamic analysis of steel plate shear wall systems, and the differential transformation method was used to solve the differential equation representing dynamic behaviour of the equivalent continuous Timoshenko beam. The development of the presented method assumed that:

- The material shows linear elastic behaviour
- The displacements are small enough so that geometric nonlinear effects can be neglected
- Structural properties can be considered uniform throughout the building height
- Torsional effects around the building's vertical axis can be neglected.

An approach based on a continuous system calculation model is developed in this study to determine dynamic characteristics of steel buildings using the SPSW system. In the literature, the continuous system calculation model has been used for free vibration analysis of such systems. In addition to calculation of natural periods, the approach developed in this study also enables calculation of the base shear force, maximum storey displacement, and maximum storey drift ratio.

2. Mathematical model of the SPSW system

The continuous system calculation model, based on idealization of structures as a cantilever beam, is one of the methods used in the static and dynamic analysis of structures. In the continuous system calculation model, depending on the structural bearing system and the importance of axial displacements, the structures can be idealized as an equivalent flexural-shear beam, shear beam, Timoshenko beam, flexural beam, and sandwich beam.

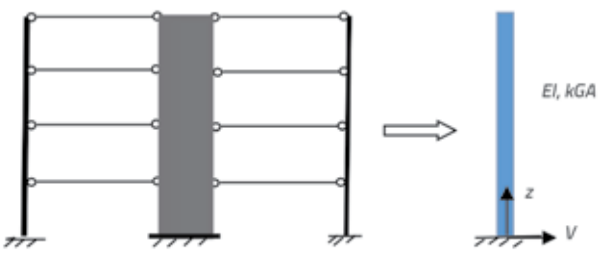

Figure 1. Steel plate wall structure idealized as a Timoshenko beam

Studies on the modelling of buildings as equivalent Timoshenko beams have been conducted in the literature [20-30]. In these studies, it was concluded that the Timoshenko beam model is suitable for the analysis and identification of regular buildings.

In this paper, the typical SPSW system is modelled as an equivalent Timoshenko beam (Figure 1).

According to the literature [21-23], the differential equation system of the Timoshenko model shown in Figure 1 is written as follows.

$$(EI)\frac{\partial^4 V_b}{\partial z^4} + \rho A \frac{\partial^2 V}{\partial t^2} = 0 \tag{1}$$

$$(kGA)\frac{\partial^2 V_s}{\partial z^2} - \rho A \frac{\partial^2 V}{\partial t^2} = 0 \tag{2}$$

where V_b is the lateral displacement due to bending, V_s is the lateral displacement due to shear, V is the total lateral displacement, z is the vertical axis up to height, (EI) is the equivalent bending stiffness of the Timoshenko beam, ρ is the unit volume weight, A is the cross-sectional area, and (kGA) is the equivalent shear stiffness.

The total lateral displacement is the sum of the lateral displacement that occurs with the bending and shear and is calculated by the following relation:

$$V = V_b + V_s \tag{3}$$

Shear force in the Timoshenko beam is calculated by the following equation:

$$(EI)\frac{\partial^3 V_b}{\partial z^3} = -(kGA)\frac{\partial V_s}{\partial z} \tag{4}$$

Equation (5) can be written with the assumption of harmonic vibration.

$$V(z,t) = y(z)\cdot e^{i\omega t}\, V_b(z,t) = y_b(z)\cdot e^{i\omega t}\, V_s(z,t) = y_s(z)\cdot e^{i\omega t} \tag{5}$$

where ω is the angular frequency.

If Equation (5) is applied in partial differential equations (1), (2), and (4), ordinary differential equations (6), (7), and (8) are obtained.

$$(EI)\frac{d^4 y_b}{dz^4} - \rho A\omega^2 y = 0 \tag{6}$$

$$(kGA)\frac{d^2 y_s}{dz^2} + \rho A\omega^2 y = 0 \tag{7}$$

$$(EI)\frac{d^3 y_b}{dz^3} = -(kGA)\frac{dy_s}{dz} \tag{8}$$

Equation (9) can be written from Equation (5).

$$y = y_b + y_s \tag{9}$$

If Equation (9) is placed in differential Equation (6), then the differential Equation (10) is obtained.

$$(EI)\left[\frac{d^4y}{dz^4} - \frac{d^4y_s}{dz^4}\right] - \rho A\omega^2 y = 0 \tag{10}$$

If the differential Equation (7) is derived twice according to *z*, Equation (11) is obtained.

$$(kGA)\frac{d^4y_s}{dz^4} + \rho A\omega^2\frac{d^2y}{dz^2} = 0 \tag{11}$$

By using the differential Equation (11), Equation (12) is obtained.

$$\frac{d^4y_s}{dz^4} = -\frac{\rho A\omega^2}{(kGA)}\frac{d^2y}{dz^2} \tag{12}$$

If the Equation (12) is written in Equation (10), Equation (13) is obtained.

$$(EI)\left[\frac{d^4y}{dz^4} + \frac{\rho A\omega^2}{(kGA)}\frac{d^2y}{dz^2}\right] - \rho A\omega^2 y = 0 \tag{13}$$

If both sides of the differential Equation (13) are divided into (EI), Equation (14) is written.

$$\frac{d^4y}{dz^4} + \frac{\rho A\omega^2}{(kGA)}\frac{d^2y}{dz^2} - \frac{\rho A\omega^2}{(EI)}y = 0 \tag{14}$$

Boundary conditions of the linear differential Equation (14) are:

a) The displacement and rotation due to bending at the base are zero
b) the bending moment and shear force at the top of structures are zero. These expressions are mathematically listed below.

$$y(0) = 0 \tag{15}$$

$$\frac{dy_b}{dz} = 0 \tag{16}$$

$$\text{za } z = H\,(EI)\frac{d^2y_b}{dz^2} = 0 \tag{17}$$

$$\text{za } z = H\,(EI)\frac{d^3y_b}{dz^3} = 0 \tag{18}$$

If necessary adjustments are made in Equations (16), (17), and (18), Equations (19), (20), and (21) are obtained.

$$\text{za } z = 0\frac{dy}{dz} + \frac{(EI)}{(kGA)}\left[\frac{d^3y}{dz^3} + \frac{\rho A\omega^2}{(kGA)}\frac{dy}{dz}\right] = 0 \tag{19}$$

$$\text{za } z = H(EI)\left[\frac{d^2y}{dz^2} + \frac{\rho A\omega^2 y}{(kGA)}\right] \tag{20}$$

$$\text{za } z = H(EI)\left[\frac{d^3y}{dz^3} + \frac{\rho A\omega^2}{(kGA)}\frac{dy}{dz}\right] = 0 \tag{21}$$

The following transformation can be done to make the given equations non-dimensional.

$$\varepsilon = \frac{z}{H} \tag{22}$$

If the transformation is applied in Equation (14), Equation, (23) is obtained.

$$\frac{1}{H^4}\frac{d^4y}{d\varepsilon^4} + \frac{1}{H^2}\frac{\rho A\omega^2}{(kGA)}\frac{d^2y}{d\varepsilon^2} - \frac{\rho A\omega^2}{(EI)}y = 0 \tag{23}$$

If both sides of the differential Equation (23) are multiplied by H^4, then the differential Equation (24) is obtained.

$$\frac{d^4y}{d\varepsilon^4} + H^2\frac{\rho A\omega^2}{(kGA)}\frac{d^2y}{d\varepsilon^2} - \frac{\rho A\omega^2H^4}{(EI)}y = 0 \tag{24}$$

If the necessary adjustment is made in Equation (24), the differential Equation (25) is written as follows:

$$\frac{d^4y}{d\varepsilon^4} + \frac{(EI)}{(kGA)H^2}\frac{\rho A\omega^2H^4}{(EI)}\frac{d^2y}{d\varepsilon^2} - \frac{\rho A\omega^2H^4}{(EI)}y = 0 \tag{25}$$

If dimensionless parameters are assigned to coefficients of the differential Equation (25), the differential Equation (26) is written.

$$\frac{d^4y}{d\varepsilon^4} + r^2a\frac{d^2y}{d\varepsilon^2} - ay = 0 \tag{26}$$

r^2 and α are non-dimensional parameters in the differential Equation (26) and are defined by the following Equations (27) and (28).

$$r^2 = \frac{(EI)}{(kGA)H^2} \tag{27}$$

$$a = \frac{\rho A \omega^2 H^4}{(EI)} \tag{28}$$

Similarly, the boundary condition (15) can be written non-dimensionally with Equation (28).

$$y(0) = 0 \tag{29}$$

The boundary condition in (19) can be written in non-dimensional form as in Equation (30).

$$Za\,\varepsilon = 0\left[1+\frac{(EI)^2}{H^4(kGA)^2}\frac{\rho A\omega^2 H^4}{(EI)}\right]\frac{dy}{d\varepsilon}+\frac{(EI)}{(kGA)H^2}\frac{d^3y}{d\varepsilon^3}=0 \tag{30}$$

If Equations (27) and (28) are written in Equation (30), Equation (31) is obtained.

$$Za\,\varepsilon = 0\left[1+r^4a\right]\frac{dy}{d\varepsilon}+r^2\frac{d^3y}{d\varepsilon^3}=0 \tag{31}$$

The boundary condition (20) is dimensionally written as follows:

$$Za\,\varepsilon = 1\frac{d^2y}{d\varepsilon^2}+\frac{\rho A\omega^2}{(EI)}H^4\frac{(EI)}{(kGA)H^2}y=0 \tag{32}$$

If Equations (27) and (28) are written in Equation (32), Equation (33) is obtained.

$$Za\,\varepsilon = 1\frac{d^2y}{d\varepsilon^2}+r^2ay=0 \tag{33}$$

If Equation (22) is applied in Equation (21), then Equation (34) is obtained.

$$Za\,\varepsilon = 1\frac{d^3y}{d\varepsilon^3}+\frac{\rho A\omega^2}{(EI)}H^4\frac{(EI)}{(kGA)H^2}\frac{dy}{d\varepsilon}=0 \tag{34}$$

If Equations (27) and (28) are written in (34), then Equation (35) is obtained.

$$Za\,\varepsilon = 1\frac{d^3y}{d\varepsilon^3}+r^2a\frac{dy}{d\varepsilon}=0 \tag{35}$$

The y function according to the differential transform method is defined as follows [31]:

$$y(\varepsilon)=\sum_{k=0}^{\infty}\frac{\varepsilon^k}{k!}\left[\frac{d^ky}{d\varepsilon^k}\right]_{\varepsilon=0} \tag{36}$$

Equation (36) can be written as follows [31].

$$y(\varepsilon)=\sum_{k=0}^{\infty}\varepsilon^kY[k] \tag{37}$$

Here, $Y[k]$ value can be expressed by the following Equation [31]:

$$Y[k]=\frac{1}{k!}\left[\frac{d^ky}{d\varepsilon^k}\right]_{\varepsilon=0};\ 0\le\varepsilon<10 \tag{38}$$

Based on the above equations, the transformation function is expressed by Equation (39) [31].

$$DT\left(\varepsilon^\alpha y^\beta\right)=\left[\prod_{i=1}^{\beta}(k-\alpha+i)\right]Y(k-\alpha+\beta) \tag{39}$$

Here, y is defined as follows.

$$y^\beta=\frac{d^\beta y}{d\varepsilon^\beta} \tag{40}$$

If transformation (39) is applied to Equation (26), Equation (41) is obtained.

$$Y[k+4]=\frac{-r^2aY[k+2]}{(k+4)(k+3)}+\frac{aY[k]}{(k+4)(k+3)(k+2)(k+1)} \tag{41}$$

Similarly, if DTM is applied to Equations (29),(31),(33) and (35), Equations (42),(43),(44) and (45) are obtained.

$$Y[0]=0 \tag{42}$$

$$Y[3]=\frac{-\left(1+r^4\right)Y[1]}{6r^2} \tag{43}$$

$$\sum_{k=0}^{\infty}(k)(k-1)Y[k]+r^2a\sum_{k=0}^{\infty}Y[k]=0 \tag{44}$$

$$\sum_{k=0}^{\infty}(k)(k-1)(k-2)Y[k]+r^2a\sum_{k=0}^{\infty}Y[k]=0 \tag{45}$$

If all Y values are written in terms of Y[1] and Y[2] using equation (41), Equation (44) and Equation (45) can be written in matrix form as:

$$A\begin{Bmatrix}Y[1]\\Y[2]\end{Bmatrix}=\begin{Bmatrix}0\\0\end{Bmatrix} \tag{46}$$

The matrix Equation (46) can be written as follows.

$$\begin{bmatrix} A(1,1) & A(1,2) \\ A(2,1) & A(2,2) \end{bmatrix} \begin{Bmatrix} Y[1] \\ Y[2] \end{Bmatrix} = \begin{Bmatrix} 0 \\ 0 \end{Bmatrix} \quad (47)$$

α values are found by nontrivial solution of the matrix Equation (47). If natural period is written instead of angular frequency in Equation (28), Equation (48) is obtained.

$$a = \frac{4\rho A\pi^2 H^4}{\mathrm{T}^2(EI)} \quad (48)$$

Using Equation (48), the natural vibration period is found as follows:

$$T_i = \frac{2\pi}{a_i} H^2 \sqrt{\frac{\rho A}{EI}} = S_i H^2 \sqrt{\frac{\rho A}{EI}} \quad (49)$$

Equation (50) is obtained from Equation (49).

$$S_i = \frac{2\pi}{a_i} \quad (50)$$

S_i values from Equation (50) are calculated for different r^2 values and are presented in Figure 2 and Table 1.

In the lumped mass calculation model, it is accepted that the masses are collected at storey levels, whereas in the continuous system calculation model the masses are considered to be distributed along the height of the building. For this reason, there are significant differences between the two calculation models, especially in low-rise buildings. The correction coefficient (Ж), which varies depending on the number of floors, is defined in order to adapt the continuous system calculation model to the lumped mass system calculation model. Accordingly, the natural period value can be calculated as follows:

$$T_i = \frac{S_i H^2}{Ж_i} \sqrt{\frac{\rho A}{EI}} \quad (51)$$

SAP 2000 was used for the calculation of correction factors. For this, the correction factor is defined through results obtained by solving the structures with varying numbers of floors, using the lumped mass calculation model with SAP 2000. The correction factors for the first three modes are given in Table 2.

Modal participation factor (Γ) based on dynamic analysis is calculated using the following Equation [32]:

$$\Gamma_i = \frac{\sum_{j=1}^{n}(m_j y_{ji})}{\sum_{j=1}^{n}(m_j y_{ji}^2)} \quad (52)$$

The effective mass ratio (*em*) can be calculated using Equation (53) [32].

$$em_i = \frac{1}{M_t} \frac{\left[\sum_{j=1}^{n}(m_j y_{ji})\right]^2}{\sum_{j=1}^{n}(m_j y_{ji}^2)} \quad (53)$$

where M_t represents the total building mass.

For the first three modes, *em* effective mass ratios are presented in Figure 3 and Table 1. The base shear force for i. mode is calculated by the following Equation[32]:

$$V_{bi} = em_i \cdot M_t \cdot S_{ai} \quad (54)$$

The peak point displacement can be calculated with the following Equation [32]:

$$d_{max}\mathrm{i} = \Gamma_i y_i(1) S_{di} = dep_i S_{di} \quad (55)$$

where S_{ai} and S_{di} stand for spectral acceleration and spectral displacement, respectively, and are calculated for the ith mode. For different r^2 values, *dep* values in the first three modes are calculated and presented in Figure 4 and Table 1.

For the maximum inter-storey drift ratio location found for the corresponding mode, the maximum inter-storey drift ratio values, corresponding to the same place in the other mode, can be calculated using Equation 56.

$$dr_{ij} = \Gamma_i \frac{1}{H}\left(\frac{dy_i(\varepsilon_{jmax})}{d\varepsilon}\right) S_{di} = \frac{\beta_{ij}}{H} S_{di}; \ \mathrm{i} = 1, 2, 3; \ \mathrm{j} = 1, 2, 3 \quad (56)$$

For the first modes, the values of β are calculated using Equation (56), and are presented in Figure 5 and Table 1.

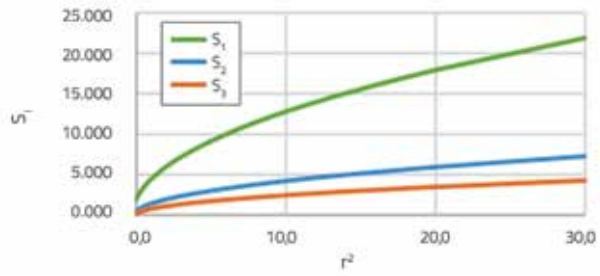

Figure 2. S values for the first three modes

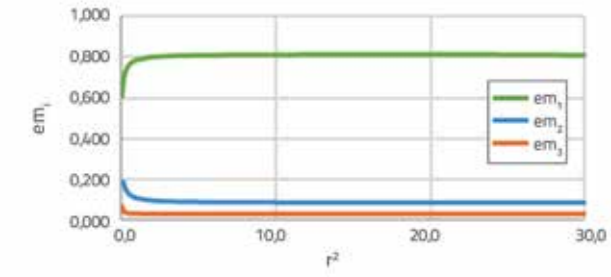

Figure 3. Effective mass ratios values

Table 1. Dynamic coefficients

r^2	S_1	S_2	S_3	em_1	em_2	em_3	dep_1	dep_2	dep_3	β_{11}	β_{21}	β_{31}
0.0	1.787	0.285	0.102	0.610	0.190	0.070	1.570	0.870	0.510	-	-	-
0.1	2.171	0.575	0.284	0.687	0.187	0.049	1.500	0.690	0.337	1.792	2.330	2.440
0.2	2.504	0.740	0.383	0.722	0.162	0.043	1.460	0.630	0.310	1.686	2.380	2.268
0.3	2.801	0.866	0.460	0.743	0.145	0.040	1.430	0.590	0.290	1.654	2.345	2.202
0.4	3.070	0.971	0.526	0.756	0.134	0.039	1.410	0.560	0.290	1.651	2.230	2.168
0.5	3.319	1.064	0.584	0.765	0.127	0.038	1.390	0.540	0.280	1.660	2.257	2.147
0.6	3.550	1.148	0.637	0.772	0.121	0.038	1.380	0.530	0.280	1.674	2.222	2.132
0.7	3.768	1.226	0.686	0.777	0.117	0.037	1.370	0.510	0.280	1.689	2.194	2.122
0.8	3.974	1.298	0.731	0.781	0.113	0.037	1.360	0.500	0.280	1.704	2.170	2.113
0.9	4.170	1.367	0.774	0.785	0.111	0.037	1.350	0.500	0.270	1.719	2.149	2.106
1.0	4.357	1.431	0.814	0.787	0.108	0.037	1.343	0.489	0.274	1.733	2.132	2.102
2.0	5.913	1.961	1.142	0.801	0.097	0.036	1.311	0.454	0.268	1.827	2.043	2.080
3.0	7.138	2.372	1.395	0.805	0.093	0.035	1.299	0.440	0.266	1.872	2.009	2.072
4.0	8.183	2.722	1.608	0.808	0.091	0.035	1.292	0.433	0.265	1.899	1.991	2.068
5.0	9.108	3.031	1.796	0.809	0.090	0.035	1.288	0.429	0.265	1.916	1.980	2.066
6.0	9.947	3.312	1.966	0.810	0.089	0.035	1.285	0.426	0.264	1.928	1.972	2.064
7.0	10.721	3.570	2.123	0.811	0.089	0.035	1.283	0.424	0.264	1.937	1.967	2.063
8.0	11.443	3.811	2.268	0.811	0.088	0.035	1.282	0.422	0.264	1.944	1.962	2.062
9.0	12.122	4.038	2.405	0.812	0.088	0.035	1.280	0.421	0.263	1.949	1.959	2.061
10.0	12.765	4.252	2.535	0.812	0.088	0.035	1.279	0.420	0.263	1.954	1.957	2.060
11.0	13.377	4.456	2.658	0.812	0.087	0.035	1.279	0.419	0.263	1.957	1.954	2.060
12.0	13.962	4.652	2.776	0.813	0.087	0.035	1.278	0.418	0.263	1.960	1.953	2.060
13.0	14.524	4.839	2.889	0.813	0.087	0.035	1.277	0.418	0.263	1.963	1.951	2.059
14.0	15.065	5.019	2.998	0.813	0.087	0.035	1.277	0.417	0.263	1.965	1.950	2.059
15.0	15.587	5.194	3.103	0.813	0.087	0.035	1.277	0.417	0.263	1.967	1.948	2.058
16.0	16.092	5.362	3.204	0.813	0.087	0.035	1.276	0.416	0.263	1.969	1.947	2.058
17.0	16.581	5.525	3.302	0.813	0.086	0.035	1.276	0.416	0.263	1.970	1.947	2.058
18.0	17.057	5.684	3.398	0.813	0.086	0.035	1.276	0.416	0.263	1.972	1.946	2.058
19.0	17.520	5.838	3.491	0.814	0.086	0.035	1.275	0.415	0.263	1.973	1.945	2.058
20.0	17.971	5.988	3.581	0.814	0.086	0.035	1.275	0.415	0.263	1.974	1.945	2.058
30.0	21.977	7.324	4.385	0.810	0.086	0.035	1.270	0.410	0.260	1.980	1.940	2.060

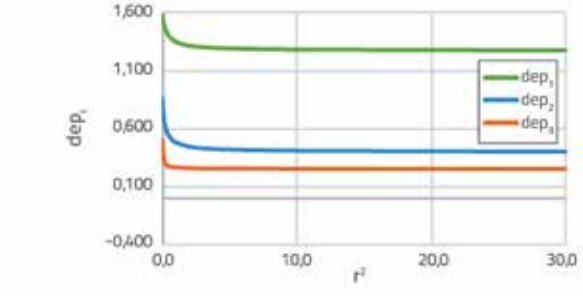

Figure 4. Displacement values for the first three modes

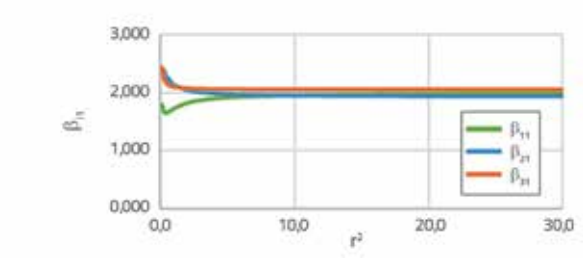

Figure 5. β values for the first mode

Table 2. Reduction coefficients

Number of floors	1. Mode	2. Mode	3. Mode
1	0.492	-	-
2	0.664	0.704	-
3	0.749	0.781	0.751
4	0.799	0.821	0.829
5	0.833	0.848	0.860
6	0.857	0.868	0.878
7	0.875	0.883	0.892
8	0.889	0.895	0.903
9	0.900	0.905	0.912
10	0.909	0.913	0.919
11	0.917	0.920	0.925
12	0.923	0.926	0.931
13	0.928	0.931	0.935
14	0.933	0.935	0.939
15	0.937	0.939	0.943
16	0.941	0.943	0.946
17	0.944	0.946	0.949
18	0.947	0.948	0.952
19	0.950	0.951	0.954
20	0.952	0.953	0.956
21	0.954	0.955	0.958
22	0.956	0.957	0.960
23	0.958	0.959	0.962
24	0.960	0.960	0.963
25	0.961	0.962	0.965
26	0.963	0.963	0.966
27	0.964	0.964	0.967
28	0.965	0.966	0.968
29	0.967	0.967	0.969
30	0.968	0.968	0.970

3. Numerical example

The plan and section of the 4-storey steel structure taken from the literature [33] are shown in Figure 6. The characteristics of the building are given in Table 3.

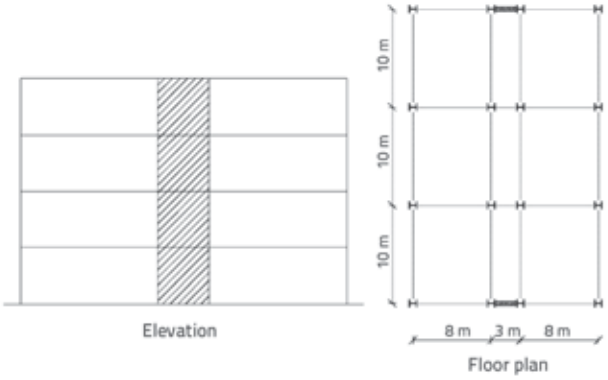

Figure 6. Floor plans of example [33]

Table 3. Properties of the building

Plate thickness	3 mm
Plate width	3 m
VBE section HD	HD 400 x 287
Number of floors	4
Floor height	3.29 m
Total building height (H)	13.16 m
Mass distributed over the height of the building (ρA)	45.593 t/m

Considering the gross moment of inertia of the system, the natural periods of the first three modes are calculated with the method presented in this study (Timoshenko beam model). The same example is modelled using SAP2000 and ETABS. The

Table 4. Natural period values

Natural periods [s]	Timoshenko Beam Model	SAP2000	ETABS	ANSYS [33]
T_1	0.606	0.569	0.586	0.563
T_2	0.181	0.158	0.159	-
T_3	0.095	0.080	0.080	-

SPSW system is modelled with shell elements in the analysis with SAP2000 and ETABS. The SAP2000 model is shown in Figure 7.

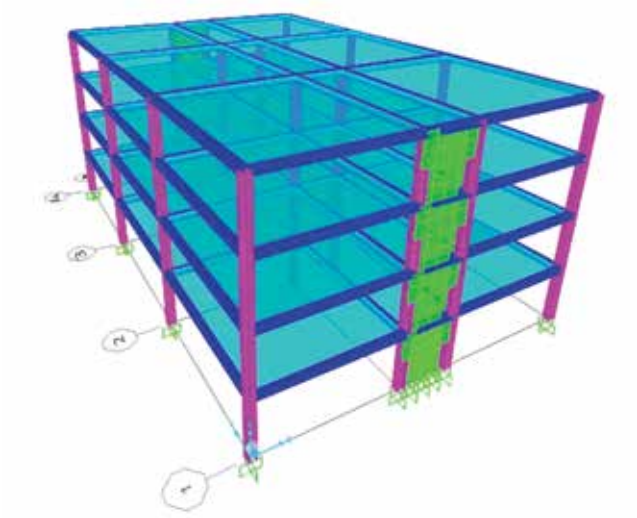

Figure 7. SAP2000 3D model

(EI) and (kGA) values calculated in the literature [32] using gross section are given below.

$(EI) = 44 \cdot 10^6$ [kNm^2]

$(kGA) = 0.902 \cdot 10^6$ [kN]

Using Equation (27), r^2 is determined as follows.

$$r^2 = \frac{44 \cdot 10^6}{0.902 \cdot 10^6 \cdot 13.16^2} = 0.282$$

For $r^2 = 0.281$ value from Table 1, the values of S_1 S_2 and S_3 are:

$S_1 = 2.746$, $S_2 = 0.843$ i $S_3 = 0.,446$

The following Ж values are found in Table 2 for a 4-storey building.

$Ж_1 = 0.799$, $Ж_2 = 0.821$ i $Ж_3 = 0.829$

Using the gross section moment of inertia, the natural periods of the first three modes are established as follows using Equation (51).

$$T_1 = \frac{2.746 \cdot 13.16^2}{0.799}\sqrt{\frac{45.593}{44 \cdot 10^6}} = 0.606 \text{ [s]}$$

$$T_2 = \frac{0.843 \cdot 13.16^2}{0.821}\sqrt{\frac{45.593}{44 \cdot 10^6}} = 0.181 \text{ [s]}$$

$$T_3 = \frac{0.446 \cdot 13.16^2}{0.829}\sqrt{\frac{45.593}{44 \cdot 10^6}} = 0.095 \text{ [s]}$$

The comparison of natural periods calculated using the gross section moment of inertia is given in Figure 8 and Table 4.

Figure 8. Comparison of natural periods calculated using the gross section moment of inertia

The response spectrum analysis of the same building is made with the Timoshenko beam model presented in this study in accordance with the Turkish Building Earthquake Code (TBEC 2018). Earthquake parameters used in the calculations are given in Table 5.

Table 5. Earthquake parameters (5 storeys)

City	Çanakkale (Turkey)
Ground motion level	DD-2
S_s	0.719
S_1	0.219
S_{DS}	0.970
S_{D1}	0.702
T_A [s]	0.145
T_B [s]	0.723
T_L [s]	6
Local site class	ZE
Seismic load reduction factor	6
Strength reduction factor	2.5

Table 6. Natural Period values (TBEC 2018)

Natural periods [s]	Timoshenko Beam Model	SAP2000	ETABS
T_1	0.615	0.699	0.704
T_2	0.184	0.202	0.202
T_3	0.097	0.102	0.101

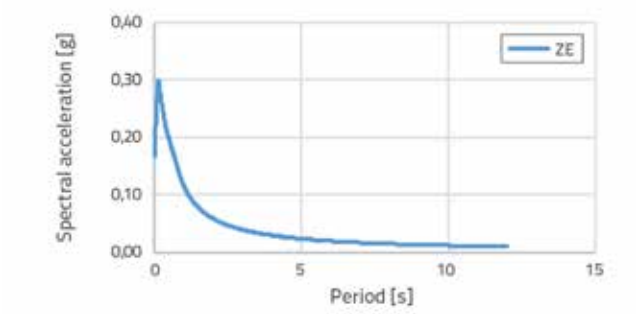

Figure 9. Reduced elastic design spectrum curve

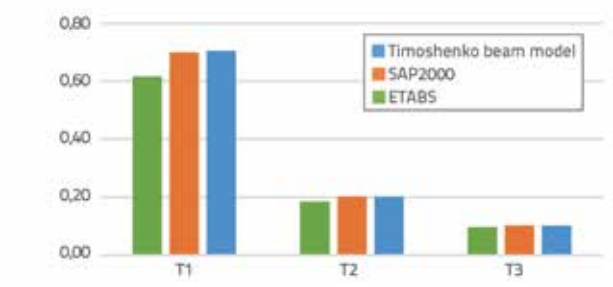

Figure 10. Comparison of natural periods calculated using the effective gross section moment of inertia

Effective cross-section stiffnesses are used while performing dynamic analysis in TBEC. The *(EI)* and *(kGA)* values calculated accordingly are given below.

$(EI) = 43.12 \cdot 10^6$ [kNm^2]

$(kGA) = 0.868 \cdot 10^6$ [kN]

Using Equation (27), r^2 can be obtained as follows:

$$r^2 = \frac{43.12 \cdot 10^6}{0.868 \cdot 10^6 \cdot 13.16^2} = 0{,}287$$

For $r^2 = 0.287$ value from Table 1, S_1 S_2 and S_3 amount to:

$S_1 = 2.762$; $S_2 = 0.849$; $S_3 = 0.450$

Ж values from Table 2 for a 4-storey building amount to:

$Ж_1 = 0.799$, $Ж_2 = 0.821$; $Ж_3 = 0.829$

With the help of Equation (51) and using the effective cross-section stiffness, natural periods of the first three modes can be obtained as follows:

$$T_1 = \frac{2.762 \cdot 13.16^2}{0.799}\sqrt{\frac{45.593}{43.12 \cdot 10^6}} = 0.615 \text{ [s]}$$

$$T_2 = \frac{0.849 \cdot 13.16^2}{0.821}\sqrt{\frac{45.593}{43.12 \cdot 10^6}} = 0.184 \text{ [s]}$$

$$T_3 = \frac{0.450 \cdot 13.16^2}{0.829}\sqrt{\frac{45.593}{43.12 \cdot 10^6}} = 0.097 \text{ [s]}$$

Natural periods calculated using the effective cross-section stiffness are given in Table 6 and Figure 10.

For $r^2 = 0.287$ value from Table 1, em_1 em_2 and em_3 amount to:

$em_1 = 0.740$; $em_2 = 0.147$; $em_3 = 0.040$

Using Figure 9, spectral acceleration values corresponding to calculated natural period values amount to:

$Sa_1 = 1{,}737$ [m/s^2]; $Sa_2 = 2{,}806$ [m/s^2]; $Sa_3 = 2{,}564$ [m/s^2]

Base shear force values for all three modes are calculated using Equation (54) and they amount to:

$V_{b1} = 0.740 \cdot 1200 \cdot 1.737 = 1542.456$ [kN]

$V_{b2} = 0.147 \cdot 1200 \cdot 2.06 = 494.978$ [kN]

$V_{b3} = 0.040 \cdot 1200 \cdot 2.564 = 123.072$ [kN]

The design base shear force can be calculated according to the square root of the sum of the squares (SRSS) method as follows:

$$V_b = \sqrt{1542.456^2 + 494.978^2 + 123.072^2} = 1624.599 \text{ [kN]}$$

For $r^2 = 0.287$ value from Table 1, dep_1 dep_2 and dep_3 amount to:

$dep_1 = 1.433983$; $dep_2 = 0.595311$ i $dep_3 = 0.292656$

Using Figure 9, spectral displacement values corresponding to calculated natural period values amount to:

$Sd_1 = 0.017$ [m]; $Sd_2 = 0.0024$ [m]; $Sd_3 = 0.00061$ [m]

Table 7. Comparison of base shear force, peak displacement, and maximum drift ratio

	Timoshenko Beam Model	SAP2000	ETABS
V_t [kN]	1624.599	1617.895	1607.402
d_{max} [m]	0.0244	0.0264	0.0268
dr_{max}	0.002187	0.002322	0.002372

The peak displacement corresponding to each of the three modes was calculated with the help of the Equation (55) as follows:

$$d_{max1} = 1.433986 \cdot 0{,}017 = 0.0244 \text{ [m]}$$

$$d_{max2} = 0.595311 \cdot 0{,}0024 = 0.0014 \text{ [m]}$$

$$d_{max3} = 0.292656 \cdot 0{,}00061 = 0.00018 \text{ [m]}$$

The design peak displacement can be calculated according to the square root of the sum of the squares (SRSS) method as follows:

$$d_{max} = \sqrt{0.0244^2 + 0.0014^2 + 0.00018^2} = 0.0244 \text{ [m]}$$

For $r^2 = 0.287$ value from Table 1, β_{11}, β_{21}, and β_{31} amount to:

$\beta_{11} = 1.6582489$; $\beta_{21} = 2.3496473$; $\beta_{31} = 2.2107634$

The maximum drift ratio corresponding to each of the three modes was calculated with the help of the Equation (56) as follows:

$$dr_{11} = \frac{1.6582489}{13.16} \cdot 0.017 = 2.142 \cdot 10^{-3}$$

$$dr_{21} = \frac{2.3496473}{13.16} \cdot 0.0024 = 4.285 \cdot 10^{-4}$$

$$dr_{31} = \frac{2.2107634}{13.16} \cdot 0.00061 = 1.025 \cdot 10^{-4}$$

The design maximum drift ratio can be calculated according to the square root of the sum of the squares (SRSS) method as follows:

$$dr_{max} = \sqrt{(2.142 \cdot 10^{-3})^2 + \left(4.285 \cdot 10^{-4}\right)^2 + \left(1.025 \cdot 10^{-4}\right)^2} = 0.002187$$

The base shear force, peak displacement, and maximum drift ratio values were calculated using the method presented in this study (Timoshenko beam model) and compared with SAP2000 and ETABS in Table 8 and in figures 11, 12, and 13.

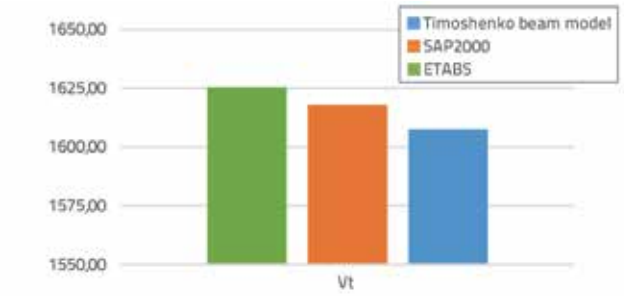

Figure 11. Comparison of base shear forces

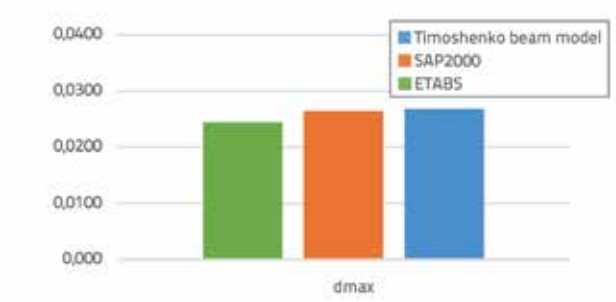

Figure 12. Comparison of maximum displacement

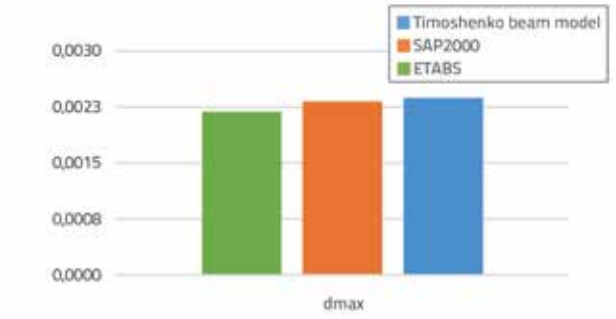

Figure 13. Comparison of maximum storey drifts

4. Conclusions

A continuous system calculation model is proposed for spectral analysis of buildings with an SPSW system is presented in this study. The SPSW system is idealized in this study as an equivalent Timoshenko beam. The mathematical model of the equivalent Timoshenko beam was solved by the differential transform method and the result was obtained. The method presented in this study is suitable for regular buildings and cannot be used as such for non-regular buildings. With the presented approach, the natural periods, base shear force, peak displacement, and maximum storey drift ratio are obtained quickly and practically. At the end of the study, it was demonstrated that the approach presented from the solved sample gave results that are sufficiently close to the finite element method. With the presented method, it is possible to obtain information about dynamic behaviour of buildings using a few parameters only. The method presented can be used in the preliminary design stage.

REFERENCES

[1] Love, R.J., Yu, K., McNeill, S., Zepeda, D.: Retrofit of a Critical Care Facility in Los Angeles with Steel Plate Shear Walls, Structures Congress 2008, Vancouver, Canada, April 2008, https://doi.org/10.1061/41016(314)103.

[2] Berman, J.W., Lowes, L.N., Baldvins, N.M., Low, N.A.: Performance-Based Design Tools for Steel Plate Shear Walls, Structures Congress 2010, Orlando, Florida, United States, May 2010, https://doi.org/10.1061/41130(369)311.

[3] Bhowmick, A.K., Driver, R.G., Grondin, G.Y.: Application of indirect capacity design principles for seismic design of steel-plate shear walls, Struct. Eng., 137 (2011) 4, pp. 521-530, https://doi.org/10.1061/(ASCE)ST.1943-541X.0000303.

[4] Clayton, P.M., Dowden, D.M., Purba, R., Berman, J.W., Lowes, L.N., Bruneau, M.: Seismic Design and Analysis of Self-Centring Steel Plate Shear Walls, Structures Congress 2011, Las Vegas, Nevada, United States, April 2011, https://doi.org/10.1061/41171(401)66.

[5] Clayton, P.M., Winkley, T.B., Berman, J.W., Lowes, L.N.: Experimental investigation of self-centring steel plate shear walls, Struct. Eng., 138 (2012) 7, https://doi.org/10.1061/(ASCE)ST.1943-541X.0000531.

[6] Alavi, E., Nateghi, F.: Experimental study of diagonally stiffened steel plate shear walls, Struct. Eng., 139 (2013) 11, pp. 1795-1811, https://doi.org/10.1061/(ASCE)ST.1943-541X.0000750.

[7] Nie, J.G., Zhu, L., Fan, J.S., Mo, Y.L.: Lateral resistance capacity of stiffened steel plate shear walls, Thin-Walled Struct., 67 (2013), pp. 155-167. https://doi.org/10.1016/j.tws.2013.01.014.

[8] Dowden, D.M., Bruneau, M.: Dynamic shake-table testing and analytical investigation of self-centring steel plate shear walls, Struct. Eng., 142 (2016) 10, https://doi.org/10.1061/(ASCE)ST.1943-541X.0001547.

[9] Dowden, D.M., Clayton, P.M., Li, C.H., Berman, J.W., Bruneau, M., Lowes, L.N., Tsai, K.C.: Full-scale pseudodynamic testing of self-centring steel plate shear walls, Struct. Eng., 142 (2016) 1, https://doi.org/10.1061/(ASCE)ST.1943-541X.0001367.

[10] Yu, J.G., Feng, X.T., Li, B., Hao, J.P.: Cyclic performance of cross restrained steel plate shear walls with transverse braces, Thin-Walled Struct., 132 (2018), pp. 250-264, https://doi.org/10.1016/j.tws.2018.08.020.

[11] Wang, X.T., Xie, C.D.: Experimental and numerical investigation of steel beam-to-cfst column frame-thin steel plate shear walls with cross stiffness, Steel Struct., 19 (2019), pp. 1895-1910, https://doi.org/10.1007/s13296-019-00253-z.

[12] Barua, K., Bhowmick, A.K.: Nonlinear seismic performance of code designed perforated steel plate shear walls, Steel and Composite Struct., 31 (2019) 1, pp. 85-98, http://dx.doi.org/10.12989/scs.2019.31.1.085.

[13] Curkovic, I., Skejic, D., Dzeba, I.: Seismic performance of steel plate shear walls with variable column flexural stiffness, Steel and Composite Struct., 33 (2019) 1, pp. 1-18, http://dx.doi.org/10.12989/scs.2019.33.1.001.

[14] Bai, J., Zhang, J., Du, K., Jin, S.: A simplified seismic design method for low-rise dual frame-steel plate shear wall structures, Steel and Composite Struct., 37 (2020) 4, pp. 447-462, http://dx.doi.org/10.12989/scs.2020.37.4.447.

[15] Azarafrooz, A., Shekastehband, B.: Behaviour of fully- connected and partially-connected multi-storey steel plate shear wall structures, Struct. Eng. and Mech., 76 (2020) 3, pp. 311-324, http://dx.doi.org/10.12989/sem.2020.76.3.311.

[16] Fathy, E.: Seismic assessment of thin steel plate shear walls with outrigger system, Struct. Eng. and Mech., 74 (2020) 2, pp. 267-282. http://dx.doi.org/10.12989/sem.2020.74.2.267.

[17] Liu, J.L., Xu, L.H., Li, Z.X.: Experimental study on component performance in steel plate shear wall with self-centring braces, Steel and Composite Struct., 37 (2020) 3, pp. 341-351, http://dx.doi.org/10.12989/scs.2020.37.3.341.

[18] Jiang, R., Jiang, L., Hu, Y., Jiang, L., Ye, J.: A simplified method for fundamental period prediction of steel frames with steel plate shear walls, The Struct. Design of Tall and Special Buildings, 29 (2020) 7, https://doi.org/10.1002/tal.1718.

[19] Zhao, Q., Qiu, J., Zhao, Y., Yu, C.: Estimating fundamental period of corrugated steel plate shear walls, Struct. Eng., 24 (2020), pp. 3023-3033, https://doi.org/10.1007/s12205-020-2305-2.

[20] Baikov, V.N., Sigalov, E.E.: Reinforced Concrete Structures, MIR Publishers, Moscow, Russia, 1981.

[21] Köpecsiri, A., Kollar, L.P.: Approximate analysis of tall building structures for earthquake using the Timoshenko-beam, Period. Polytech. Civ. Eng., 42 (1998) 2, pp. 139-162.

[22] Rahgozar, R., Safari, H., Kaviani, P.: Free vibration of tall buildings using timoshenko beams with variable cross-section, In Proceesings of SUSI VIII, Crete, Greece, pp. 233-243, 2004, Doi 10.2495/SU040231.

[23] Boutin, C., Hans, S., Ibraim, E., Roussillon, P.: In situ experiments and seismic analysis of existing buildings—Part II: Seismic integrity threshold, Earth. Eng. Struct. Dyn., 34 (2005) 12, pp. 1531-1546, https://doi.org/10.1002/eqe.503.

[24] Ebrahimian, M., Todorovska, M.I.: Structural system identification of buildings by a wave method based on a nonuniform Timoshenko beam model, J. Eng. Mech., ASCE, 141 (2015) 8, https://doi.org/10.1061/(ASCE)EM.1943-7889.0000933.

[25] Cheng, M.H., Heaton, T.H.: Simulating building motions using ratios of the building's natural frequencies and a Timoshenko beam model, Earth. Spectra, 31 (2015) 1, pp. 403-420, https://doi.org/10.1193/011613EQS003M.

[26] Su, R.K.L., Tang, T.O., Liu, K.C.: Simplified seismic assessment of buildings using non-uniform Timoshenko beam model in low-to-moderate seismicity regions, Eng. Struct., 120 (2016), pp. 116-132, https://doi.org/10.1016/j.engstruct.2016.04.006.

[27] Taciroglu, E., Ghahari, S.F., Abazarsa, F.: Efficient model updating of a multi-storey frame and its foundation stiffness from earthquake records using a Timoshenko beam model, Soil Dyn. And Earth. Eng., 92 (2017), pp. 25-35, https://doi.org/10.1016/j.soildyn.2016.09.041.

[28] Ozmutlu, A., Ebrahimian, M., Todorovska, M.I.: Wave propagation in buildings as periodic structures: Timoshenko beam with rigid floor slabs model, J. Eng. Mech., 144 (2018) 4, https://doi.org/10.1061/(ASCE)EM.1943-7889.0001436.

[29] Feretti, M.: Flexural torsional buckling of uniformly compressed beam-like structures, Continuum Mech. Thermodyn., 30 (2018), pp. 977-993, https://doi.org/10.1007/s00161-018-0627-9.

[30] Feretti, M., D'Annibale, F.: Buckling of tower buildings on elastic foundation under compressive tip forces and self-weight, Continuum Mech. Thermodyn., (2020), https://doi.org/10.1007/s00161-020-00911-2.

[31] Rajasekaran, S.: Structural Dynamics of Earthquake Engineering: Theory and Application using Mathematica and Matlab, Woodhead Publishing in Materials, CRC Press, India, 2009.

[32] Paz, M., Kim, Y.H.: Structural Dynamics: Theory and Computation, Springer International Publishing, 2019.

[33] Topkaya, C., Kurban, C.O.: Natural periods of steel plate shear wall systems, Const. Steel Research, 65 (2009) 3, pp. 542-551, https://doi.org/10.1016/j.jcsr.2008.03.006.